

Combating cisplatin-resistant lung cancer using a coiled-coil lipopeptides modified membrane fused drug delivery system

Wang, X.; Liu, G.; Pu, X.; Ren, T.; Zhang, F.; Shen, M.; ...; Yang, J.

Citation

Wang, X., Liu, G., Pu, X., Ren, T., Zhang, F., Shen, M., ... Yang, J. (2025). Combating cisplatin-resistant lung cancer using a coiled-coil lipopeptides modified membrane fused drug delivery system. *Journal Of Controlled Release*, *379*, 45-58. doi:10.1016/j.jconrel.2025.01.004

Version: Publisher's Version

License: Licensed under Article 25fa Copyright Act/Law (Amendment Taverne)

Downloaded from: https://hdl.handle.net/1887/4281731

Note: To cite this publication please use the final published version (if applicable).



Contents lists available at ScienceDirect

Journal of Controlled Release

journal homepage: www.elsevier.com/locate/jconrel





Combating cisplatin-resistant lung cancer using a coiled-coil lipopeptides modified membrane fused drug delivery system

Xi Wang a,b,c,1 , Guiquan Liu a,b,c,1 , Xueyu Pu a,b,c,1 , Tangjun Ren a,b,c , Fan Zhang a,b,c , MengJie Shen d , Yan Zhu a,b,c , Alexander Kros d,** , Jian Yang a,b,c,*

- ^a State Key Laboratory of Component-based Chinese Medicine, Tianjin University of Traditional Chinese Medicine, Tianjin 301617, China
- ^b Institute of Traditional Chinese Medicine, Tianjin University of Traditional Chinese Medicine, Tianjin 301617, China
- ^c Haihe Laboratory of Modern Chinese Medicine, Tianjin 301617, China
- d Leiden Institute of Chemistry-Supramolecular and Biomaterial Chemistry, Leiden University, Einsteinweg 55, 2333CC Leiden, the Netherlands

ARTICLE INFO

Keywords: Membrane fused drug delivery system Coiled-coil lipopeptide Drug-resistant lung cancer Cisplatin

ABSTRACT

Drug resistance to chemotherapy in treating cancers becomes an increasingly serious challenge, which leads to treatment failure and poor patient survival. Drug-resistant cancer cells normally reduce intracellular accumulation of drugs by controlling drug uptake and promoting drug efflux, which severely limits the efficacy of chemotherapy. To overcome this problem, a membrane fused drug delivery system (MF-DDS) was constructed to treat cisplatin (DDP)-resistant lung cancer (A549-DDP) by delivering DDP via membrane fusion using a complementary coiled-coil forming peptides (CP_8K_4/CP_8E_4). The lipopeptide CP_8K_4 was pre-incubated firstly and decorated on the surface of A549-DDP cells, and then the cells interacted with the lipopeptide CP_8E_4 modified on the lipid bilayer (LB) coated PLGA nanoparticles loading DDP (PLGA-DDP@LB- CP_8E_4), leaded to the direct cytosolic DDP delivery and cancer cell death. Compared with free DDP, this MF-DDS achieved a 13.42-folds reduced IC_{50} value of A549-DDP cells $in\ vitro$, and tumor size was down-regulated, showing only 1/5.26 of the original weight $in\ vivo$. Meanwhile, the anti-drug resistant mechanism was explored, where the MF-DDS inhibited the expression of efflux protein genes, including MRP1, MRP2, and ABCG2, leading to increased intracellular drug accumulations. Altogether, this MF-DDS effectively delivered DDP into DDP-resistant cancer cells, making it a promising and improved pharmacological therapeutic approach for drug-resistant tumor treatment.

1. Introduction

Chemotherapy, as a commonly used treatment for lung cancer, typically involves the use of chemotherapy drugs such as cisplatin (DDP), which is the first platinum chemotherapeutic drug approved by the Food and Drug Administration (FDA) to treat multiple cancers [1,2]. DDP exerts anticancer effects on non-small cell lung cancer (NSCLC), and its most prominent action is DNA damage, which further induces cell apoptosis [3]. However, prolonged or inappropriate use of anticancer drugs can lead to the acquisition of resistance by cancer cells, thereby reducing the efficacy of cancer treatment [4]. DDP resistance in

chemotherapy involves multiple mechanisms, including reducing intracellular drug accumulation by cancer cells through reducing drug uptake and facilitating drug efflux, increasing drug inactivation and DNA repairment [5,6].

General solutions to drug resistance in chemotherapy are based on earlier detection of tumors, adaptive monitoring during therapy, improved pharmacological principles, and recognition of cancer cell dependence [7]. Based on the improved pharmacological principles, nano-drugs, especially nanoparticle-based drug delivery systems (NDDs), have been proven recently to result in more effective responses, including tumor cell targeting, decreased side effects, and lessoned

E-mail addresses: a.kros@chem.leidenuniv.nl (A. Kros), yang.j2017@tjutcm.edu.cn (J. Yang).

^{*} Corresponding author at: State Key Laboratory of Component-based Chinese Medicine, Tianjin University of Traditional Chinese Medicine, Tianjin 301617, China.

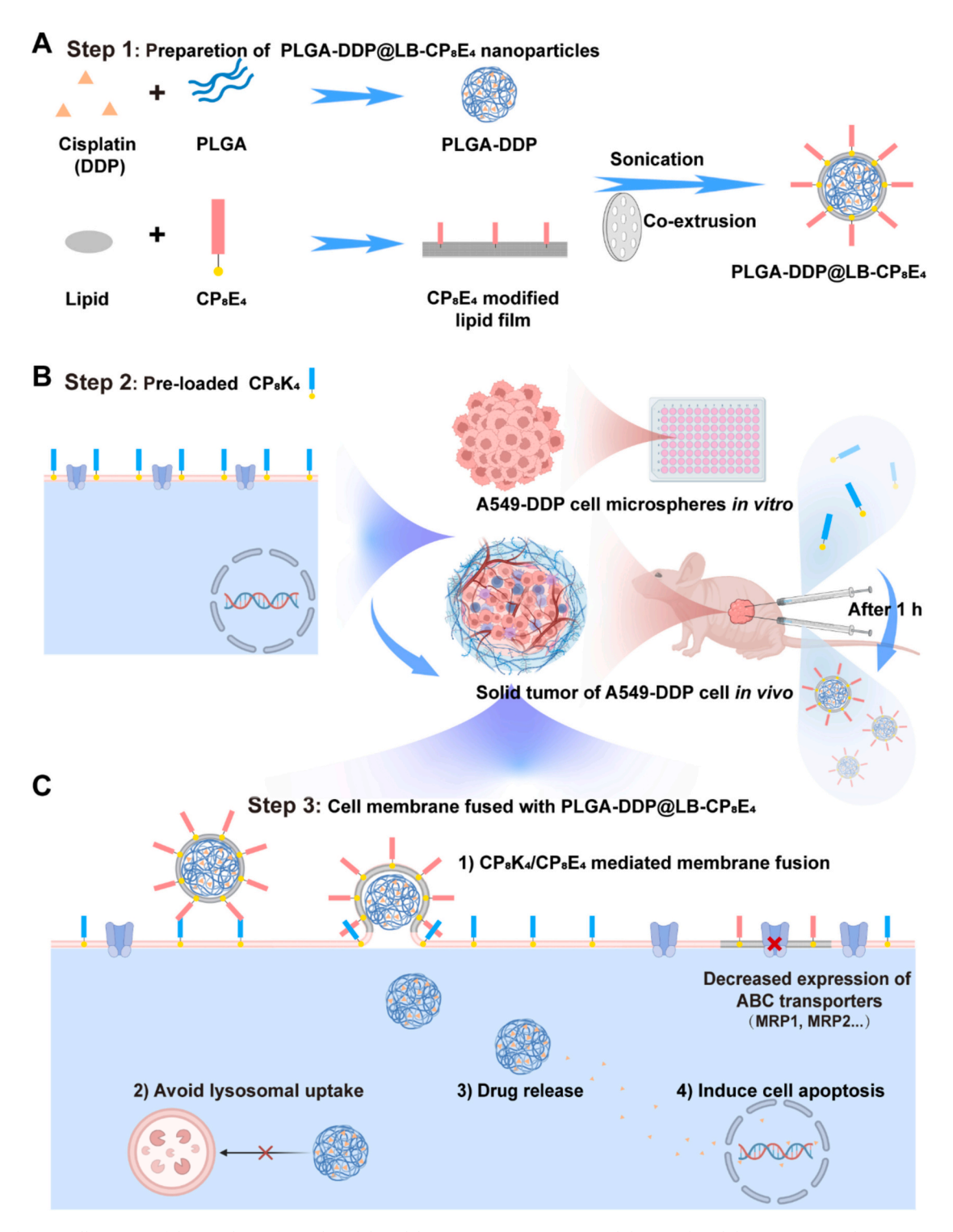
^{**} Corresponding author.

 $^{^{1}}$ Xi Wang, Guiquan Liu, and Xueyu Pu contributed equally to this work.

chemoresistance [8,9]. To address different mechanisms of DDP resistance, NDDs have been designed and used to treat DDP-resistant tumors with a diagnostic and therapeutic focus on reversing drug resistance [10,11]. For instance, Cao et al. prepared self-assembled cationic NDDs consisting of polyethylene glycol block polylactic acid, hydrophobic polylactic acid cisplatin precursor, and cationic lipids, which significantly improved cellular uptake of DDP *via* enhanced endocytosis and

reversal of DDP resistance [12]. He et al. constructed a lipid coated nanoscale coordination polymer nanoparticles loaded with DDP and siRNA that target multidrug resistance (MDR) genes to down-regulate MDR gene expression to inhibit DDP efflux, thereby increasing the synergistic therapeutic of chemotherapy [13].

Endocytosis, as a traditional entry route for NDDs that can be encapsulated by lysosomes and degraded by biological enzymes, leads to



Scheme 1. Schematic illustration of the membrane fusion-based drug delivery system preparation and then combated the DDP-resistant lung cancer. (A) Step 1: the preparation process of lipopeptide CP_8E_4 modified DDP drug delivery system (PLGA-DDP@LB- CP_8E_4). (B) Step 2: lipopeptide CP_8K_4 was pre-incubated with living cells in vitro, and the CP_8K_4 was pre-injected around the tumor for 1 h, then the PLGA-DDP@LB- CP_8E_4 was injected around the tumor in vivo. (C) Step 3: the membrane fusion drug delivery process mediated by CP_8K_4/CP_8E_4 and the mechanism relating to the expression of ABC transporters were explored.

the inactivation of the loads [14]. To overcome this problem, we previously designed a functionalized system containing cholesterol-coupled pegylated peptides K and E (CPK and CPE) with strong interaction force. We firstly anchored the positively charged CPK on the cell membrane of cancer cells and modified CPE on liposome, which delivered the drugs through form the coiled-coil peptides with strong interaction mediated membrane fusion instead of disrupting the integrity of the biological membrane, achieving the membrane fusion in cancer cells and in vivo model, showed much higher lysosome escape and drug delivery efficiency compared with traditional intracellular pathway, which further leads to high rate of cancer cell apoptosis [15-18]. Poly(lactic-co-glycolic acid) (PLGA) is one of the most successfully developed biodegradable polymers approved by the FDA, which was suitable for constructing drug delivery systems loaded with all types of drugs like hydrophilic or hydrophobic small molecules, or macromolecule drugs, which suitable for loading DDP with poor water solubility (about 1 mg/ mL) and low lipophilicity [19,20]. It was the first time to apply this drug delivery system to against drug-resistant cancer.

Here, we constructed PLGA nanoparticles loaded with DDP and lipidcoated to fuse with the cell membrane. As shown in Scheme 1, we constructed a lipopeptide-modified MF-DDS that greatly enhanced the intracellular accumulation of DDP based on complementary coiled-coil forming peptides (CP8K4/CP8E4). Firstly, CP8E4 was modified on lipid film and subsequently coated on the surface of PLGA nanoparticles loaded with DDP to constitute a functionalized lipopeptide-modified lipid bilayer (LB) coated DDP delivery system (PLGA-DDP@LB-CP8E4) (Step 1), then CP8K4 with a positive charge was pre-incubated and loaded on the surface of the A549-DDP cell membrane (Step 2). After lipopeptides recognition, binding, and internalization, the DDP was significantly delivered and the delivering mechanism was explored, resulting in cell apoptosis of DDP-resistant cancer cells in vitro and in vivo (Step 3). This approach improved the efficiency of drug-resistant cancer cell killing and held a promising therapeutic strategy for drug-resistant cancers.

2. Experimental section

2.1. Materials

Poly(lactic-co-glycolic acid) (PLGA, P133293), N,N-Dimethylformamide (DMF, D112000), Ethyl acetate (EA, E116136), Dichloromethane (CH₂Cl₂, D116146), Methanol (MeOH, M116118), and o-phenylenediamine (o-PDA, P103813) were obtained from Aladdin (Shanghai, China). Polyvinyl alcohol (PVA, 363170) was obtained from VETEC (USA). 1,2-dioleoyl-sn-glycero-3-phosphocholine (DOPC, 850375P), Dioleoyl phosphoethanolamine (DOPE, 850725P), Cholesterol (CHO, 228111), and 1,2-distearoyl-sn-glycero-3-phosphoethanolamine-N-(7nitro-2-1,3-benzoxadiazol-4-yl)(ammonium (DOPE-NBD, 810145P) were obtained from Avanti Lipid (Alabaster, USA). Cisplatin (DDP, HY-17394), Doxorubicin hydrochloride (DOX, HY-15142), Propidium iodide (PI, HY-D0815), Rhodamine 123 (Rhod-123, HY-D0816), Wortmannin (HY-10197), Chlorpromazine (HY-12708), Genistein (HY-14596), Nocodazole (HY-13520), and Cell Counting Kit-8 (CCK-8, HY-K0301) was obtained from MedChemExpress (Madison, USA). Lyso-Tracker Green DND-26 (C1047S) was obtained from Beyotime (China). Annexin V-FITC/PI Apoptosis kit (K2003) was obtained from APExBIO (Houston, USA). Modified Hematoxylin-Eosin (H&E) staining kit (G1121) and Hoechst 33342 (C0031) were obtained from Solarbio Science & Technology (Beijing, China). Ki67 monoclonal antibody (ab16667) and Alexa Fluor 488-conjugated donkey anti-rabbit antibody (ab150075) were obtained from Abcam (Cambridge, MA, USA). A one-step TUNEL in situ apoptosis kit (E-CK-A320, Green, FITC) was obtained from Elabscience (China). The cell culture products were all obtained from GIBCO (Grand Island, USA).

2.2. Preparation of CP₈E₄ modified lipid bilayer coating drug-loaded PLGA nanoparticles (PLGA@LB-CP₈E₄)

We used the O/W solvent evaporation method to prepare PLGA nanoparticles, which was described with some modifications [21]. 0.5 mL 10 mg PLGA solution (Ethyl acetate as solvent) was mixed with 0.5 mL 2 % PVA aqueous solution (wt%), then an ultrasound cell crusher was used to emulsify for 5 min (4 s on, 6 s off) at 70 W. Subsequently, nitrogen blowing was used to remove the organic solvent. The obtained dry film was resuspended with 1 mL PBS, and the final concentration was 5 mg/mL.

The DDP-loaded PLGA nanoparticles (PLGA-DDP), DOX-loaded PLGA nanoparticles (PLGA-DOX), and PI-loaded PLGA nanoparticles (PLGA-PI) were used the W/O/W solvent evaporation method. First of all, 0.5 mL 2 mg/mL DDP, 0.5 mL 1 mg/mL DOX, or 0.5 mL 1 mg/mL PI aqueous solution was mixed with 0.5 mL 10 mg/mL PLGA (Ethyl acetate as solvent), respectively, then an ultrasound cell crusher was used to emulsify for 5 min (4 s on, 6 s off) at 70 W. Subsequently, the 0.5 mL 2 % PVA aqueous solution (wt%) was added and then emulsified for 5 min (4 s on, 6 s off) at 70 W. After that, nitrogen blowing was used to remove the organic solvent and samples were stored at 4 $^{\circ}$ C for further use.

The lipid film was prepared as described [22]. Dissolved DOPC, DOPE, CHO, and CP_8E_4 in a molar ratio of 49.5: 24.75: 24.75: 1 (mol/mol) in a mixed solvent of $\text{CH}_2\text{Cl}_2\text{-MeOH}$ (2:1, v/v) to form a lipid film under the atmosphere of nitrogen. After that, the 1 mM CP_8E_4 modified lipid film was added to 5 mg/mL PLGA, PLGA-DDP, PLGA-DOX, or PLGA-PI in 4 mL deionized water, respectively, which was mixed and treated ultrasonically in the water bath for 10 min. Subsequently, the mixture was repeatedly extruded through liposome extruders (Avanti Lipid, Alabaster, USA) with the pore size of 400 to 200 nm polycarbonate porous membranes in turns for 20 times. Finally, the samples were centrifuged at 12,000 rpm for 10 min in 4 °C conditions and then stored at 4 °C for further use.

2.3. Nanoparticle characterization

Dynamic light scattering (DLS, Malvern instruments, ZEN3600, UK) was used to acquire the hydrodynamic diameter, polydispersity index (PDI), and surface charge of nanoparticles. Transmission electron microscopy (TEM, Fei, TECNAI, G2, F20, USA) was used to examine the morphology of the nanoparticles. Thermal gravimetric analyzer (TGA, TGA55, USA) was used to quantitatively analyze the modification of the LB and CP_8E_4 .

2.4. Lipid mixing assay

The lipid mixing assay was as described [16]. The CP₈E₄-decorated lipid bilayer had no fluorescent labels, while the CP8K4-decorated lipid bilayer was loaded with DOPE-NBD and DOPE-LR in a molar ratio of DOPC: DOPE: CHO: DOPE-NBD: DOPE-LR = 49.5: 24.75: 24.75: 0.5: 0.5 mol%. Then, the lipid bilayer was coated on the surface of PLGA or drugloaded PLGA nanoparticles that used the method in part "2.2.". The 0 % value was determined by measuring DOPE-NBD emission of 100 µL fluorescent-labeled PLGA@LB-CP $_8$ K $_4$ to which was added 100 μ L PBS buffer. The F(t) was the fluorescence intensity that 100 µL fluorescentlabeled PLGA@LB-CP8K4 (The preparation method was consistent with part "2.2." that replaced CP₈E₈ with equimolar CP₈K₈) was mixed with PLGA@LB-CP₈E₄ at time t (measured every 30 s for 30 min). The 100 % value was determined using PLGA@LB-CP8K4 and PLGA@LB-CP8E4, which all contained half the concentrations of DOPE-NBD and DOPE-LR (0.25 mol%). The percentage of fluorescence increase (%F(t)) is calculated with the following equation:

%F(t) = (F(t)-F0) / (Fmax-F0) (1-1).

And the fluorescence intensity was continuously and closed detected by a microplate reader (TECAN, groedig, Austria).

2.5. Encapsulation efficiency and release characteristic

We used the o-phenylenediamine (o-PDA) colorimetric assay to determine the DDP concentrations [23]. The 300 μ L DDP solution was added into an equal amount of 2 mg/mL o-PDA solution (DMF as solvent), then heated to 100 $^{\circ}$ C in a metal bath for 10 min. Finally, the absorbance at 703 nm was detected by a microplate reader. The content of DDP was calculated according to the standard curve, and the encapsulation efficiency (EE%) of DDP was further calculated with the following equation:

EE% = 100 - Abs703 after centrifuge/Abs703 before centrifuge \times 100 (1–2).

The release characteristics of DDP in PLGA-DDP@LB-CP $_8E_4$ were determined at 37 $^{\circ}C$ for 0–48 h in 50 mL PBS buffer with magnetic stirring. 1 mL dissolution medium was removed and 1 mL fresh PBS buffer was added. The release characteristics of DDP were further calculated with the following equation:

$$Xn (\%) = Cn \times V \times D/W \times 100 \% (1-3).$$

 $X (\%) = Xn + (X1 + X2 + \cdots Xn-1) \times Vi/V (1-4).$

Xn is the degree of released DDP at different time points, Cn is the concentration of DDP measured per time point, V is the volume of the total release medium, D is the dilution factor, W is the initial DDP dosage, X is the cumulative release degree, and Vi is the volume of the release medium took out for per time point.

2.6. Cell culture

Human lung cancer cell lines A549 and cisplatin-resistant human lung cancer cell lines A549-DDP were incubated in Roswell Park Memorial Institute 1640 medium (RPMI-1640) supplemented with 10 % heat inactivated fetal bovine serum (FBS) at 37 $^{\circ}\text{C}$ in humectant conditions that contained 5 % CO₂ and 95 % air. The culture medium for A549-DDP cells was also supplemented with 2 $\mu\text{g/mL}$ DDP to maintain drug resistance.

2.7. Construction of A549-DDP cell microspheres

A549-DDP cells were seeded in ultra-low adsorption 96-well U-plates at cell numbers of 1000 per well. Subsequently, 96-well U-plates were centrifuged at 1000 rpm for 1 min and cultured in 37 $^{\circ}$ C, 5 $^{\circ}$ CO₂ humectant conditions for 4 days to form A549-DDP cell microspheres, while replaced the old medium with fresh medium every two days.

2.8. Evaluation of P-glycoprotein (P-gp) function using rhodamine 123 (Rhod-123) efflux assay

We compared the retention of Rhod-123 in A549 and A549-DDP cells per unit of time as a functional indicator for the evaluations of P-gp activity [24]. A549-DDP and A549 cells were seeded into a 96-well black plate for 24 h, 3 μM Rhodamine 123 incubated with cells for 0.5, 1, 2, and 4 h. After that, we washed the cells with warm PBS buffer three times and incubated with Hoechst 33342 for 10 min. The Operetta High Content Analysis (HCA) system (PerkinElmer, Boston, MA, USA) obtained the visual images and then quantified them with Image J software.

2.9. Cytotoxicity measurement

A549-DDP cells were seeded into a 96-well plate for 24 h, then incubated for another 24 h with a concentration range from 0 to 5 μM of CP8K4, and from 0 to 1000 $\mu g/mL$ of PLGA, PLGA@LB, and PLGA@LB-CP8E4. In the group of CP8K4 + PLGA@LB-CP8E4, the 2.5 μM CP8K4 was incubated with cells for 30 min and then incubated with 0 to 1000 $\mu g/mL$ of PLGA@LB-CP8E4 for 24 h. Then the medium was removed and cells were washed three times with warm PBS buffer. Subsequently, cells were incubated with 100 μL fresh culture medium that contained 10 μL

CCK8 solution at 37 $^{\circ}$ C for 2 h. Finally, the absorbance at 450 nm was detected by a microplate reader.

2.10. Membrane fusion measurement

The DOX-PLGA and PI-PLGA nanoparticles were coated with the molar ratio of 1 % NBD-PE labeled on the surface of lipid bilayer (LB), respectively. There were 6 groups: (1) CP₈K₄ + PLGA-DOX@LB-CP₈E₄ or PLGA-PI@LB-CP₈E₄ group; (2) CP₈K₄ + PLGA-DOX@LB or PLGA-PI@LB group; (3) CP₈K₄ + PLGA@LB-CP₈E₄ + free DOX or free PI group; (4) PLGA-DOX@LB-CP₈E₄ or PLGA-PI@LB-CP₈E₄ group; (5) PLGA-DOX@LB or PLGA-PI@LB group, and (6) free DOX or free PI group. Firstly, a medium that contained 2.5 μ M CP₈K₄ was incubated with A549-DDP cells or A549-DDP cell microspheres for 30 min, then washed cells three times with fresh medium, and these nanoparticles or free drug were incubated with cells for 30 min. Subsequently, cells were washed three times with fresh medium and fixed with 4 % paraformaldehyde for 15 min at room temperature, followed by treating with Hoechst 33342 for 15 min. The HCA system obtained the visual images and quantified with Image J software.

2.11. Lysosome colocalization study

A549-DDP cells were seeded on a cell glass sheet and then treated with CP₈K₄ for 30 min, and then PLGA-DOX@LB-CP₈E₄ were incubated with cells for 0.5, 2, 6, and 12 h, respectively, and 5 nM LysoTracker DND-26 was incubated with cells for 30 min. After that, the cells were fixed with 4 % paraformaldehyde for 15 min and then incubated with Hoechst 33342 for 15 min. The images were observed by an upright fluorescence microscope (Leica THUNDER, Germany). We used the PCC and MOC values to evaluate lysosome colocalization [25,26]. PCC (Pearson correlation coefficient): value can be -1 to +1, +1 indicates perfect correlation, -1 indicates perfect but negative correlation, 0 indicates the absence of a relationship. MOC (Mande's overlap coefficient): value can be 0 to 1, where 1 indicates complete overlap and 0 indicates complete separation.

2.12. Examination of DOX distribution inside A549-DDP cell microspheres

To observe the distribution of DOX in A549-DDP cell microspheres after delivery DOX. We prepared PLGA-DOX@LB and PLGA-DOX@LB-CP₈E₄, then performed the experiments according to the steps and groups of "2.10. Membrane fusion measurement". Subsequently, A549-DDP cell microspheres were sectioned to obtain cell microsphere sections and labeled nuclei. The distribution of DOX in the cell microsphere sections was observed by an inverted fluorescence microscope (Leica Microsystems CMS GmbH ErnstLeitz-Str.17–37, Germany).

2.13. Endocytosis inhibition measurements

A549-DDP cells and A549-DDP cell microspheres were incubated with 40 μM nocodazole, 0.25 μM wortmannin, 40 μM chlorpromazine, or 200 μM genistein in the medium, respectively. After 3 h preincubation with these endocytosis inhibitors, cells were treated with CP8K4 for 30 min in the presence of inhibitors. Subsequently, cells were washed three times with fresh medium and then PLGA-DOX@LB-CP8E4 was incubated for 30 min in the presence of inhibitors. The control group was treated with inhibitors and PLGA-DOX@LB-CP8E4 without pre-incubation with CP8K4. Then, cells were washed, fixed with 4 % paraformaldehyde for 15 min, and incubated with Hoechst 33342 for 15 min. The HCA system obtained the visual images and quantified with Image J software.

2.14. Quantitative real-time polymerase chain reaction (qRT-PCR)

A549-DDP cells were treated with CP $_8$ K $_4$ for 30 min and then PLGA-DOX@LB-CP $_8$ E $_4$ for 12 and 24 h, the control group was incubated with the medium. After that, according to the manufacturer's protocol, total RNA samples from the A549-DDP cells were extracted using TRIzol® reagent (15596018CN, Invitrogen). Then, the Nanodrop 2000 was used to quantify RNA concentrations. Subsequently, the RNA samples were reverse transcribed into complementary DNA (cDNA) using TransScript One-Step gDNA Removal and cDNA Synthesis SuperMix (AT341–02, TransGen Biotech, Beijing, China). cDNA amplification was performed using the LightCycler 480 (Roche) with PerfectStart® Green qPCR SuperMix (AQ601–01-V2, TransGen Biotech, Beijing, China). The sequences of primers for qRT-PCR were listed in Table S1.

2.15. Living/dead cell staining

There were five groups: (1) Control group; (2) free DDP group; (3) PLGA-DDP@LB-CP_8E_4 group; (4) CP_8K_4 + PLGA-DDP@LB group; (5) CP_8K_4 + PLGA-DDP@LB-CP_8E_4 group. A549-DDP cells or A549-DDP cell microspheres were incubated with 2.5 μ M CP_8K_4 for 30 min, then washed cells and incubated these nanoparticles or free drug were with cells for 24 h. After that, 2 μ M Calcein-AM and 4.5 μ M PI were coincubated with these A549-DDP cells or cell microspheres for 20 min at room temperature. At last, the HCA system obtained the visual images.

2.16. Apoptosis experiments

The A549-DDP cell microspheres were treated with the MF-DDS for 24 h, and the groups were the same as the part of "2.15. living/dead cell staining". After that, microspheres were collected and digested using trypsin at 37 °C for 5 min, gently blow to obtain single-cell suspension and then washed cells. After that, the Annexin V-FITC/PI apoptosis kit was used to label cells and detected cells by flow cytometry (AFC2, Invitrogen, Carlsbad, CA, USA.) and quantified by Flowjo V10 software.

2.17. A549-DDP tumor-bearing nude mice model

BALB/c nude mice (4 weeks, 16-18 g, male) were purchased from the SPF (Beijing) biotechnology (Beijing, China). The mice were kept in Tianjin University of Traditional Chinese Medicine Animal Centre, conducting experiments by the rearing environment of the breeding room and the ethical system stipulated by the Animal Ethics Committee. After 1 week of adaptive feeding, A549-DDP cells (5 \times 10⁶ cells in 100 μL cold PBS buffer) were injected subcutaneously into the right flanks of each mouse. When the tumor grew to 100 mm³ (Tumor volume = $(L \times I)$ W^2) \times 1/2, Length (L) and width (W)), mice were further random divided into five groups (n = 5 per group) as follows: 1) Control group, 2) free DDP group, 3) CP₈K₄ + PLGA-DDP@LB group, 4) PLGA-DDP@LB-CP8E4 group, and 5) CP8K4 + PLGA-DDP@LB-CP8E4 group. Mouse in groups 3) and 5) were injected 125 μL 1 mM CP₈K₄ PBS buffer solution per mouse by peritumoral injection method, and mice in other groups were injected with an equal amount of PBS buffer, after 1 h, the free DDP or DDP-loaded nanoparticles were injected at the dose of 1 mg/ kg DDP by the peritumoral injection method at the same sites every 7 days for 3 weeks, the tumor volume and mouse body weight were recorded every 3 days. In the end, the mice were euthanized to obtain tumor tissue and then fixed, dehydrated, and sliced for later use. All animal experiments were carried out by the guidelines of the Institution Animal Care and Use Committee of Tianjin University of Traditional Chinese Medicine.

2.18. H&E staining

The H&E staining was used to observe the pathological structure of

tumors. Tumor tissue sections were dewaxed, stained with hematoxylin for 30 s, differentiated in a 1 % hydrochloric acid ethanol (v/v) solution for 1 s, blue with bluing solution for 5 s, and dye with eosin for 90 s. Meanwhile, the slices required 60 of running water flushing after each step. Finally, the tumor tissue slices were observed using an inverted fluorescence microscope.

2.19. Tunel staining

One-step TUNEL *in situ* apoptosis kit was used to label the apoptotic cells in the tumors, and we followed the steps described in the manual. Tumor tissue sections were dewaxed, penetrated cells, tunel staining working solution was used to label apoptotic cells and labeled nucleus. At last, the tumor tissue slides were observed by an upright fluorescence microscope and quantified using Flowjo V10 software.

2.20. Immunofluorescence staining

The tumor tissue sections were prepared rid of paraffin, used the 0.2 % Triton-X 100 for 10 min, followed by subjecting to antigen retrieval, and blocked the nonspecific antibody bindings for 1.5 h. Subsequently, the sections were incubated with the Ki67 monoclonal antibody (1:250) at 4 $^{\circ}\text{C}$ overnight, and incubated with the Alexa Fluor® 647-conjugated donkey anti-rabbit antibody (1:500) for 1.5 h at 37 $^{\circ}\text{C}$, and then incubated with Hoechst 33342 for 5 min at 37 $^{\circ}\text{C}$. Finally, the tumor tissue sections were observed by an upright fluorescence microscope and quantified using Image J software.

2.21. Biosafety evaluation in vivo

We determined the acute toxicity of the MF-DDS due to the fact that the MF-DDS can deliver a large amount of drugs into cells in a short period of time. So, a 3-folds dose was selected over the pharmacodynamic evaluation experiments in vivo. All healthy BALB/c nude mice were randomly divided into two groups (n = 5 per group): the control group and the $CP_8K_4 + PLGA@LB-CP_8E_4$ group. The mice in the CP_8K_4 + PLGA@LB-CP₈E₄ group were injected 125 μL 3 mM CP₈K₄ PBS buffer solution per mouse by subcutaneous injection into the right flanks. Meanwhile, the mice in the control group were injected with an equal amount of PBS buffer using the same method. After 1 h, 3-folds dose (compared with the dose of pharmacodynamic evaluation in vivo) of PLGA@LB-CP8E4 nanoparticles in 125 μ L PBS buffer or the same amount of PBS buffer in the control group was subcutaneously injected, respectively. Mouse body weights were recorded every 24 h, and the mice were euthanized and obtained the major organs at 48 h, including the heart, liver, spleen, lung, and kidney, were collected to calculate the organ index (organ weight / body weight) and for H&E staining.

2.22. Statistical analysis

All data were expressed as mean \pm SD from at least three independent experiments. The differences between the two groups were analyzed for significance (p < 0.05) by t-test or by one-way analysis of variance when more than two groups were compared. All analyses used GraphPad (GraphPad Prism 10, San Diego, CA, United States).

3. Results

3.1. Preparation and characterizations of PLGA@LB-CP₈E₄

We prepared the CP_8E_4 modified lipid bilayer (LB) coating PLGA nanoparticles (PLGA@LB-CP₈E₄) and observed them under transmission electron microscopy (TEM). TEM result showed the classic core-shell structure of PLGA@LB-CP₈E₄ in Fig. 1A. The lipid film was uniformly coated on the surface of PLGA, indicating the feasibility of the preparation process. Subsequently, the hydrodynamic diameter,

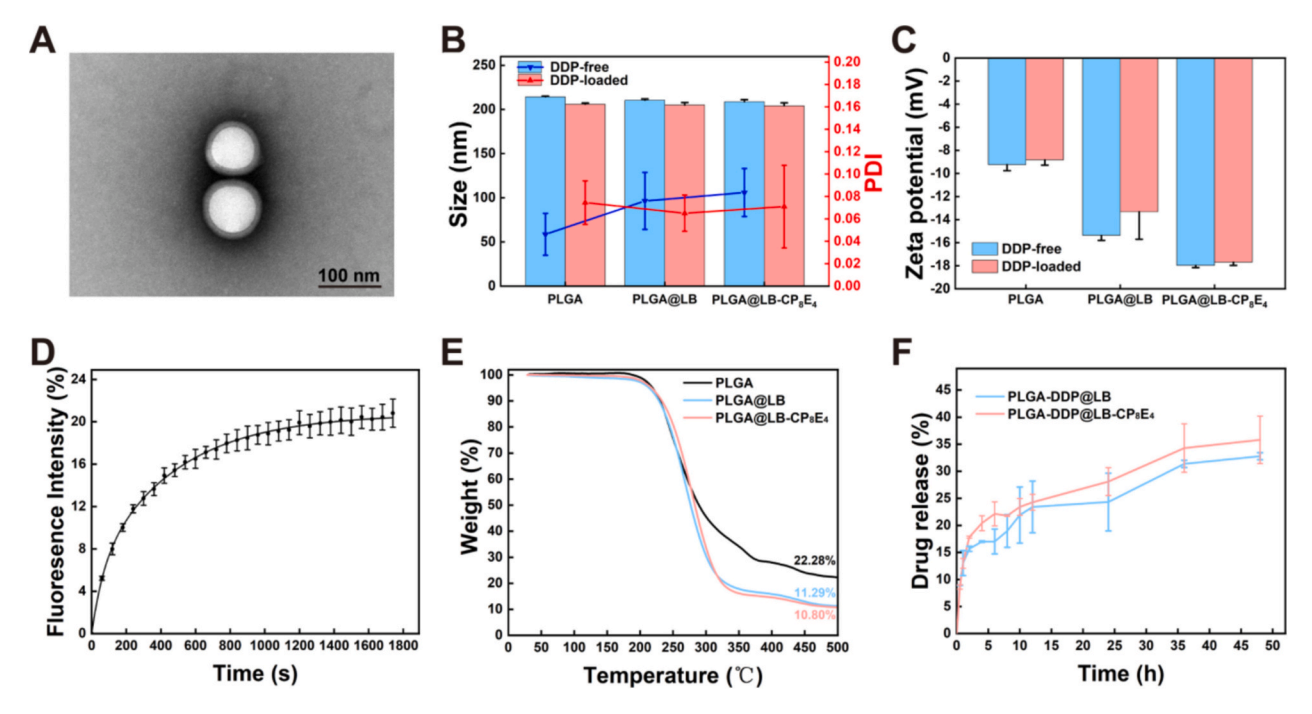


Fig. 1. Characterizations of nanoparticles. (A) The TEM image of PLGA@LB-CP $_8E_4$, scare bar = 100 nm. (B) DLS measured the size, polydispersity index (PDI), and (C) surface charge of PLGA, PLGA@LB, and PLGA@LB-CP $_8E_4$ with (DDP-loaded) or without (DDP-free) loaded with DDP. (D) Lipid mixing between PLGA@LB-CP $_8E_4$ and PLGA@LB-CP $_8E_4$. The number on the y-axis represents the percentage increase of fluorescence (from DOPE-NBD) due to liposome membrane fusion as incubated time increases. (E) The thermal gravimetric analysis of PLGA, PLGA@LB, and PLGA@LB-CP $_8E_4$. The number on the y-axis represents the percentage decrease in sample weight due to temperature increases as time increases. (F) DDP release curves of PLGA-DDP@LB and PLGA-DDP@LB-CP $_8E_4$. Values shown are mean \pm S.D., the experiment was performed in three replicates.

polydispersity index (PDI), and surface charge of PLGA, PLGA@LB, and PLGA@LB-CP₈E₄ with/without DDP were determined and compared by dynamic light scattering (DLS) (Fig. 1B,C). The size of nanoparticles was around 210 nm, marginally affected after lipid coating and lipopeptide modification, and all the PDI values were less than 0.1, indicating that all the synthesis nanoparticles had a narrow size distribution. It is worth mentioning that the surface charge was lower after lipid coating on the surface of PLGA, modification of CP₈E₄ with a negative charge further reduced the surface charge of the nanoparticles (Fig. 1C). Subsequently, we examined the particle size stability of PLGA@LB-CP₈E₄ (Fig. S1A) and PLGA-DDP@LB-CP₈E₄ (Fig. S1B), which were dispersed in deionized water, PBS buffer, and RPMI-1640 medium in 15 days. The slight size changes of PLGA@LB-CP₈E₄ and PLGA-DDP@LB-CP₈E₄ nanoparticles showed high stability.

In our previous study, a lipid mixing assay using the lipopeptide CP₄E₄/CP₄K₄ modified liposomes or solid lipid nanoparticles showed great fusogenicity [16,27]. To verify whether the lipopeptide CP₈E₄/ CP₈K₄ modified LB coated PLGA nanoparticles possess fusigenicity, the fluorescence resonance energy transfer (FRET) assay was conducted [28]. The surface charge of PLGA@LB-CP8K4 was elevated compared with PLGA@LB, which indicated the successful positive charged CP8K4 peptide modification (Table S2). Results showed that the fluorescence intensity of DOPE-NBD was increased, indicating lipid fusion occurred and the load of DDP did not affect the lipid fusion (Fig. 1D and S2). Next, a thermal gravimetric analyzer (TGA) was used to determine the modification mass percentages of the LB and CP8E4 for the PLGA and PLGA@LB, respectively (Fig. 1E). The PLGA nanoparticles remained 22.28 % weight at 500 °C, and the remained of PLGA@LB was 11.29 %, indicating that 10.99 % weight of LB was coated onto the surface of PLGA. The PLGA@LB-CP₈E₄ remained 10.80 % weight, which implied that 0.49 % weight of CP₈E₄ was modified on the PLGA@LB.

We used the o-phenylenediamine (o-PDA) colorimetric assay to detect the concentrations of DDP [23], and the encapsulation efficiency (EE%) of DDP in PLGA@LB-CP $_8$ E4 was 21.26 \pm 3.72 %. The release

curve of DDP was time-dependent, with about 23.42 \pm 4.77 % of DDP released at 12 h and 32.78 \pm 0.65 % at 48 h for PLGA-DDP@LB, and the modification of CP8E4 did not affect the release of DDP (Fig. 1F). In conclusion, we have successfully constructed a coiled-coil lipopeptides modified DDP loaded MF-DDS with high stability.

3.2. Intracellular drug delivery via membrane fusion in DDP-resistant cancer cell model in vitro

We first identified the fluorescence intensity of Rhod-123 in A549-DDP and A549 cells, the indicator of P-glycoprotein (P-gp) activity relating to drug resistance [24]. The result showed that the fluorescence intensity of Rhod-123 in A549-DDP cells was significantly lower than in A549 cells at each time point, indicating that A549-DDP cells have more expression of P-gp activity that could accelerate drug efflux (Fig. S3). After incubation with DDP, the IC $_{\!50}$ value of A549-DDP cells (25.9 $\mu g/$ mL) was significantly higher than A549 cells (5.88 $\mu g/$ mL) (Fig. S4). The results demonstrated that the A549-DDP can be used as drug-resistant cancer cells for further study.

To investigate whether CP_8E_4 and CP_8K_4 could promote membrane fusion between the lipid bilayer and living A549-DDP cell membrane. Since DDP shows non-fluorescent, we chose a fluorescently anti-tumor model drug, doxorubicin (DOX), in the subsequent visualization study, which is also a water-soluble and small molecule chemotherapeutic agent that targets DNA in the nucleus for chemotherapy [29]. Meanwhile, we used propidium iodide (PI) for further verification, which is a DNA-intercalating fluorescent dye, cell membrane of living cells was impermeable and stained DNA only when cell membrane integrity was disrupted [30]. The PLGA-DOX@LB-CP_8E_4 and PLGA-PI@LB-CP_8E_4 showed slightly changed of larger size and PDI value, and similar surface charge compared with PLGA@LB-CP_8E_4 (Fig. S5 and Table S2). Also, FRET results showed that this coiled-coiled lipopeptides-mediated membrane fusion was not affected after PLGA loading with DOX (Fig. S5E,F).

Subsequently, we examined the coiled-coil lipopeptides modified MF-DDS ($CP_8K_4 + PLGA@LB-CP_8E_4$) on cells. A549-DDP cells were preincubated with CP_8K_4 for 30 min before being incubated with the fluorescence labeling $PLGA@LB-CP_8E_4$ for 30 min. The core of PLGA contained the DOX or PI with red-fluorescent, and the coated LB labeled DOPE-NBD lipid with green-fluorescent to localize the LB. The red-fluorescent was observed in the cytoplasm and nucleus, and the green fluorescence from the DOPE-NBD was observed on the cell membrane at

the same time, indicating that membrane fusion and the content release had occurred (Fig. 2A(a) and Fig. S6A). However, the results of the control group showed an inconspicuous fluorescence signal of DOX or PI in the cytoplasm and DOPE-NBD labeled cell membrane when CP_8K_4 or CP_8E_4 lipopeptides were omitted, indicating that these two peptides mediated membrane fusion are strictly required (Fig. 2A(b,d) and Fig. S6B,D). To further rule out the possibility that the membrane fusion process leads to transient membrane instability that would allow the free

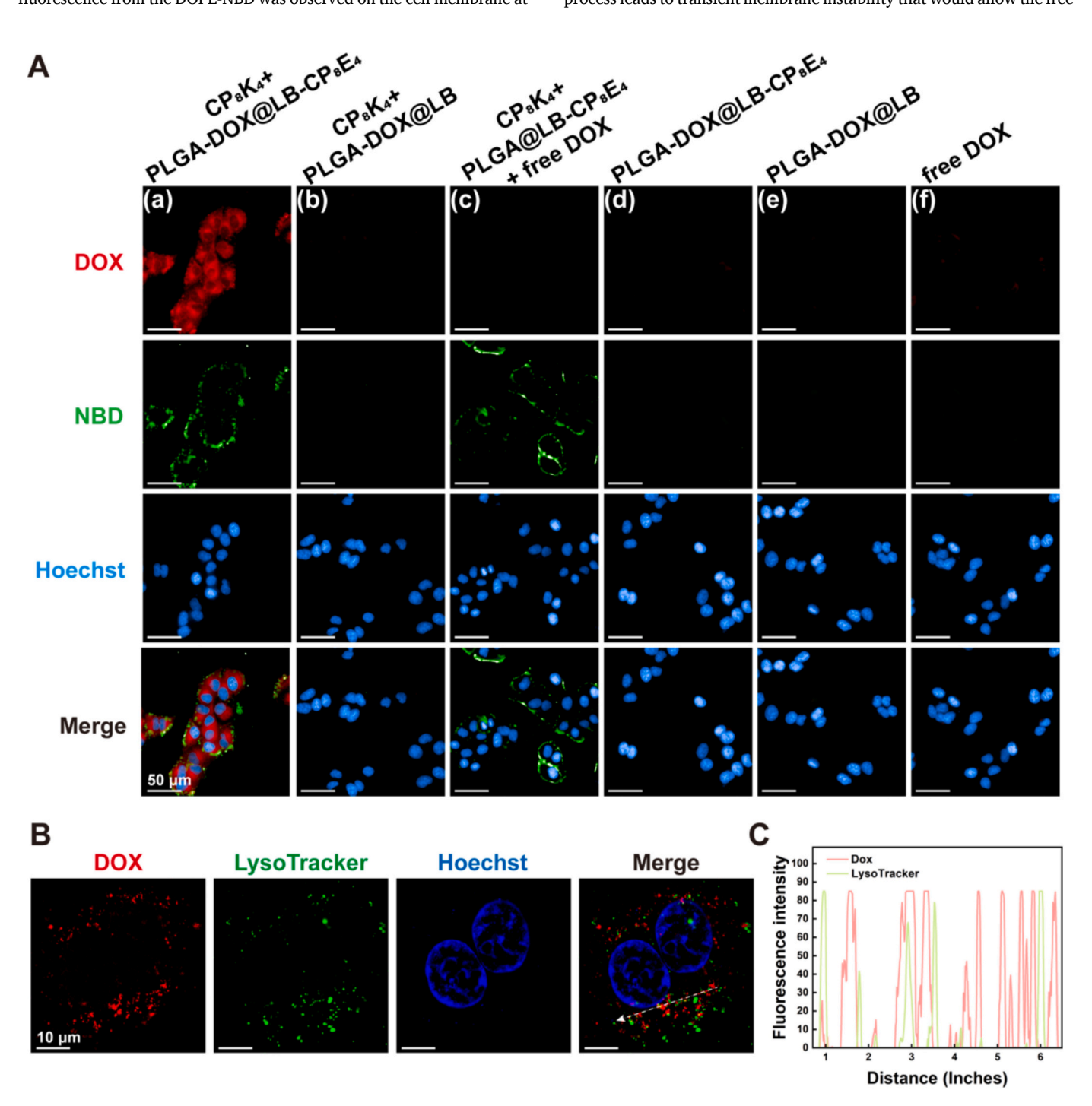


Fig. 2. Delivery of DOX by membrane fusion on A549-DDP cells. (A) Images of A549-DDP cells that were (a,b,c) pre-incubated with CP_8K_4 or (d,e,f) medium for 30 min, removed medium and washed three times with fresh medium, followed by treatment with (a,d) DOPE-NBD labeled PLGA-DOX@LB- CP_8E_4 , (b,e) DOPE-NBD labeled PLGA-DOX@LB, (c) DOPE-NBD labeled PLGA@LB- CP_8E_4 plus free DOX, and (f) free DOX for 30 min. DOX (red channel, Ex/Em = 490/590 nm), DOPE-NBD (green channel, Ex/Em = 460/534 nm), and Hoechst 33342 (blue channel, Ex/Em = 346/460 nm). Scale bar = 50 μ m. (B) Confocal images of the A549-DDP cells incubated with CP_8K_4 for 30 min, then incubated with PLGA-DOX@LB- CP_8E_4 for 30 min, the lysosome was labeled using a lyso-tracker DND-26 (green channel, Ex/Em = 504/511 nm) and nucleus were labeled using Hoechst 33342. Scale bar = 10 μ m. (C) Quantitative co-localization analysis of DOX and lysosomes in the dashed arrow area of the merge channel as a function of time using Image J.

drug to enter cells. The control group of the CP₈K₄-treated A549-DDP cells, after incubated with the PLGA@LB-CP₈E₄ and free DOX or PI, could only clearly observe the fluorescence of DOPE-NBD on the cell membrane (Fig. 2A(c) and Fig. S6C). Also, a feeble fluorescence signal was observed in the group of PLGA-DOX@LB or PLGA-PI@LB modified with DOPE-NBD and the group of free DOX or PI when all of the two lipopeptides were omitted (Fig. 2A(e,f) and Fig. S6E,F). Drug-loaded nanoparticles usually enter cells *via* the endocytosis pathway, which often fails to escape lysosomal phagocytosis and results in low delivery efficiency. Subsequently, we used the MF-DDS to deliver the DOX and simultaneously labeled lysosomes. As shown in Fig. 2B, we observed that almost all the DOX fluorescence signals could not be co-localized with

lysosomal fluorescence signals. And we calculated the Pearson correlation coefficient (PCC) was 0.28 and the Mander's overlap coefficient (MOC) was 0.362, they were both used to quantify the degree of colocalization between fluorophores [25,26]. In addition, partial DOX signals can be observed in the nucleus after 2 h delivery and an increased DOX fluorescence signal can also be observed in the nucleus with increasing time, and the low PCC and MOC values indicated that the MF-DDS can avoid uptake by lysosomes (Fig. S7).

The 3D cell culture system can narrow the gap between 2D cell and animal models by simulating complex cell heterogeneity and interactions, as well as tumor microenvironment conditions more closely and overcome the limitations of traditional 2D cell models [31].

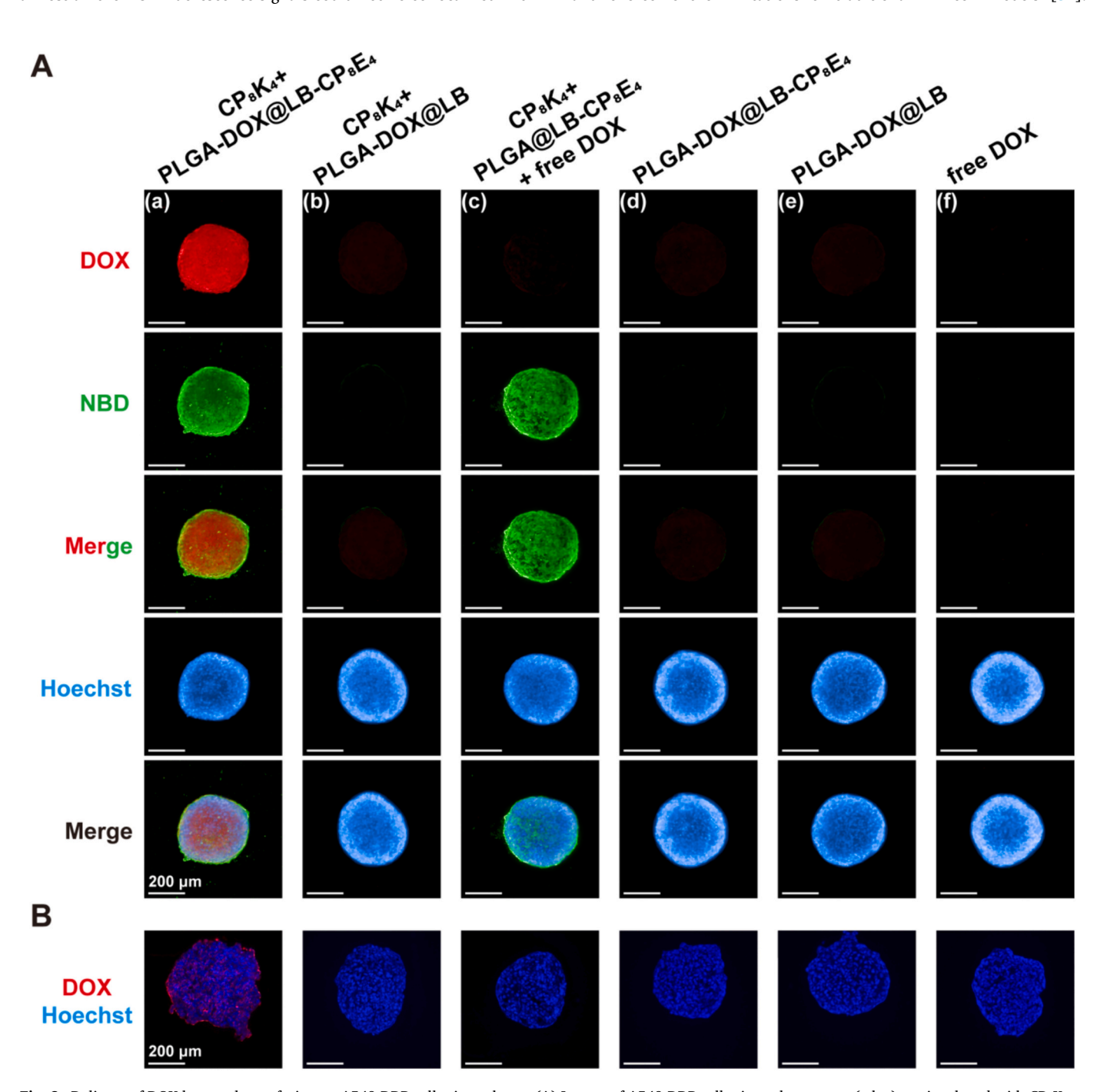


Fig. 3. Delivery of DOX by membrane fusion on A549-DDP cell microspheres. (A) Images of A549-DDP cell microspheres were (a,b,c) pre-incubated with CP_8K_4 or (d,e,f) medium for 30 min, removed medium and washed three times with fresh medium, and then followed by treatment with (a,d) DOPE-NBD labeled PLGA-DOX@LB-CP₈E₄, (b,e) DOPE-NBD labeled PLGA-DOX@LB-CP₈E₄ plus free DOX, and (f) free DOX for 30 min. (B) Slicing sections of A549-DDP cell microspheres after being treated with CP_8K_4 for 30 min and then treated with PLGA-DOX@LB-CP₈E₄ for 30 min. Scare bar = 200 μm.

Therefore, we constructed a DDP-resistant 3D lung cell microsphere model using A549-DDP cells in vitro to mimic the lesion microenvironment of the tumor. Cell microspheres were also incubated with CP8K4 for 30 min before being incubated with the DOPE-NBD labeled PLGA-DOX@LB-CP₈E₄. As shown in Fig. 3A, the fluorescence result showed that the DOPE-NBD labeled on the lipid coating appeared in the outermost part of the cell microsphere. In contrast, the PLGA-loaded DOX appeared in the inner part of the cell microsphere. Consistent with the results of membrane fusion in the 2D cell model, the other control groups showed feeble DOX fluorescence signals, further proving that MF-DDS effectively delivers drugs in the 3D model. Similarly, the inner structure of sections of 3D cell microspheres was also performed. We found a higher DOX fluorescence intensity in the outermost cells of the 3D cell microspheres and a homogeneous DOX distribution inside the 3D cell microspheres (Fig. 3B). Quantitative results showed that there was no significant difference in the uptake of DOX by cell microspheres in the non-membrane fusion mediated DOX delivery group. Importantly, the MF-DDS allowed 10.69-folds DOX accumulations in the cell microspheres compared with the free DOX group (Fig. S8). These results demonstrated that the MF-DDS could deliver a large amount of DOX into cells in a short time and showed much higher delivery efficiency than the endocytosis pathway, and the membrane fusion delivery of drugs can largely avoid the uptake by lysosomes and penetrate into the interior of the cancer cell microspheres.

3.3. Cell uptake mechanism of MF-DDS in DDP-resistant cancer cell model

To further demonstrate that membrane fusion is the primary mechanism of our drug delivery system, several well-characterized inhibitors (nocodazole, wortmannin, chlorpromazine, and genistein) of inhibiting endocytotic pathways were tested. Wortmannin, a selective PI3K inhibitor, inhibits micropinocytosis [32], nocodazole as a microtubule formation inhibitor used to inhibit intracellular trafficking [33], chlorpromazine inhibits lattice-protein-mediated endocytosis [34], and genistein inhibits caveola-dependent endocytosis [35]. In the 2D cell culture

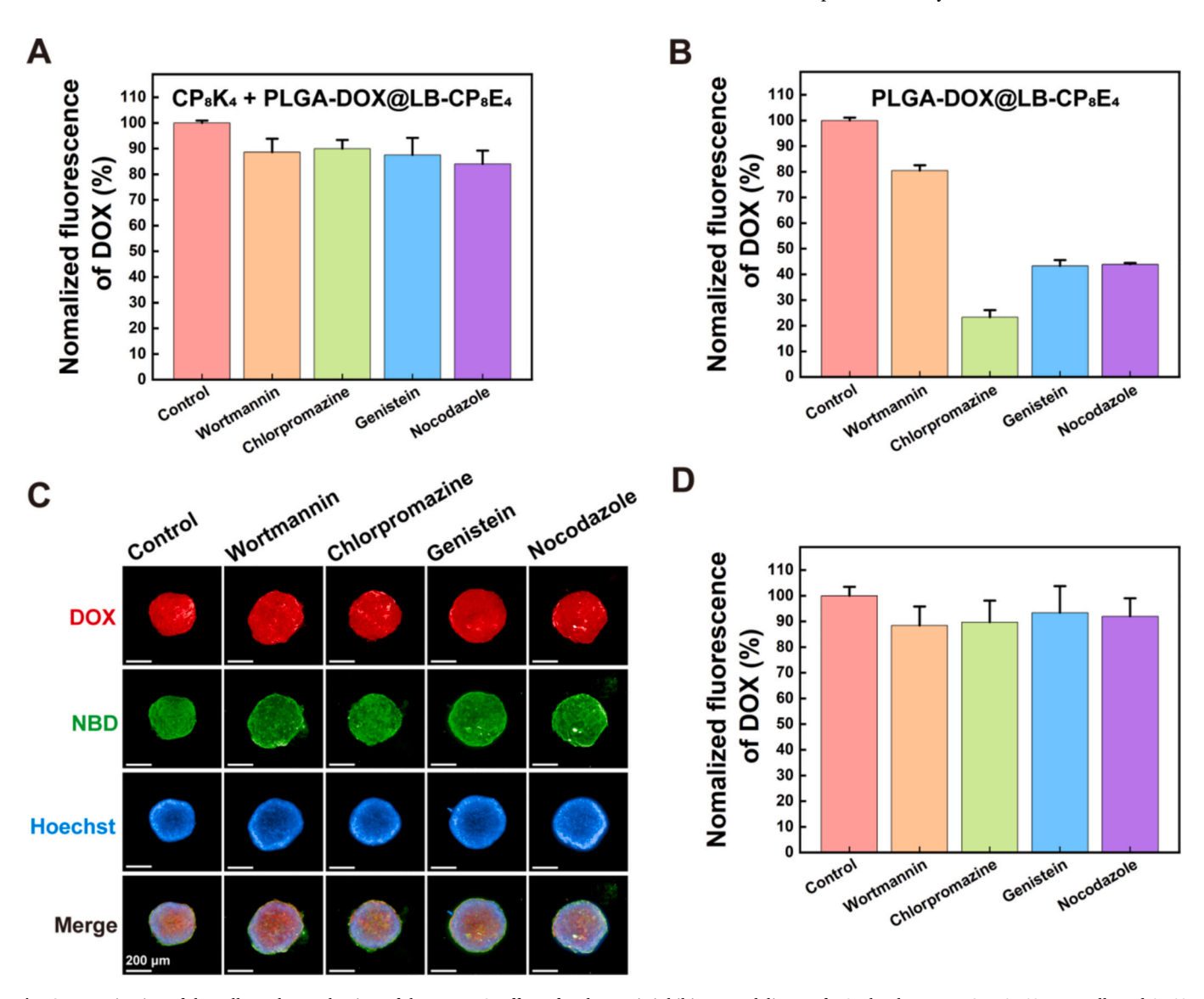


Fig. 4. Investigation of the cell uptake mechanism of the MF-DDS. Effect of endocytosis inhibitors on delivery of DOX by the MF-DDS to A549-DDP cells and A549-DDP cell microspheres. Cells were incubated with medium (Control), or medium containing 0.25 μM wortmannin, 40 μM chlorpromazine, 200 μM genistein, or 40 μM nocodazole for 3 h, then incubated with (A) CP_8K_4 or (B) fresh medium for 30 min in the presence of inhibitors, and then treated PLGA-DOX@LB- CP_8E_4 for 30 min. Cellular uptake was measured by the HCA system and the results were normalized with the control group. (C) Images and (D) quantification of DOX uptake in A549-DDP cell microspheres in the presence of endocytosis inhibitors after the A549-DDP cell microspheres that pre-incubated with CP_8K_4 for 30 min, and then incubated with DOPE-NBD labeled PLGA-DOX@LB- CP_8E_4 for 30 min. Scale bar = 200 μm, n = 6, values shown are mean \pm S.D.

model, A549-DDP cells were pre-incubated with each inhibitor for 3 h, and then cells were incubated with CP_8K_4 for 30 min, and then treated with PLGA-DOX@LB- CP_8E_4 for 30 min. The results showed that the DOX uptake by A549-DDP cells showed a slight effect by these inhibitors (Fig. 4A). However, the PLGA-DOX@LB- CP_8E_4 delivery system without pre-incubated with CP_8K_4 and the use of endocytosis inhibitors inhibited the delivery of DOX, and lattice-protein induced endocytosis was the major delivery approach (Fig. 4B).

Next, the inhibitors mentioned above were used to block the corresponding endocytosis pathways in the DDP-resistant 3D lung cancer cell microsphere, under the conditions of CP_8K_4 and CP_8E_4 intro action systems (Fig. 4C,D). The green fluorescence of NBD presented on the surface of the microsphere, while the red fluorescence of DOX mainly showed inside of the microspheres could still be observed after using the endocytosis inhibitors. The inhibitors did not interfere with the progress of membrane fusion, and the quantitative results demonstrated that membrane fusion showed the primary role in the uptake of drugs in the MF-DDS, which was consistent with the results in the 2D cell model. These results further supported that the dominant pathway for intracellular delivery of MF-DDS was *via* direct membrane fusion between the lipid membrane and the cell membrane of living cancer cells.

3.4. The expression of efflux receptor genes was inhibited after membrane fused delivery

Cancer cells upregulate the expression of related drug transporters in response to sustained stimulation of chemotherapy drugs, further leading to the development of drug resistance in cancer cells, with a particular focus on the over-expressed ATP-binding cassette (ABC) transporter proteins mediated drug efflux mechanism, mainly includes MDR1 (P-glycoprotein, P-gp), multidrug resistance-associated proteins (MRPs), lung drug resistance proteins (LRPs), and breast cancer resistance proteins (BCRPs, ABCG2) that were normally high expressed on the NSCLC cell line [36,37]. Therefore, we examined whether this MF-DDS mediated fusion of artificial lipid membranes and cell membranes would affect the expression of ABC transporter proteins, including MDR1, MDR2, MRP1 (ABCC1), MRP2 (ABCC2), LRP, and ABCG2 in A549-DDP cells after the membrane fused with PLGA@LB-CP8E4 for 12 and 24 h. Interestingly, results showed that membrane fusion could significantly reduce gene expression of ABC transporter proteins like MRP1 at 24 h (Fig. S9A). Meanwhile, the gene expression of MRP2 and ABCG2 at 12 h was significantly decreased compared with the control group (Fig. S9B,C). No significant changes were observed in the expression of other ABC transporter proteins-related genes, such as MRD1, MRD2, and LRP (Fig. S9D—F). This may be due to the membrane fusion led to a large accumulation of artificial lipids in the cell within a short period and affected lipid metabolism reprogramming, which in turn reduced the expression of drug-resistant genes and against drug resistance in cancer cells [38,39]. Altogether, this result suggested that this MF-DDS synergistically combated DDP-resistant lung cancers by rapidly delivering the drug while decreasing the expression of efflux receptors.

3.5. The killing capability of the MF-DDS with DDP-resistant lung cancer cell model in vitro

The artificial lipid membrane we prepared will fuse with the cell membrane, and due to the positively charged $\mathrm{CP_8K_4}$ lipopeptide, this may lead to cell death. Therefore, we investigated the impact of $\mathrm{CP_8K_4}$ and non-drug loaded MF-DDS on the viability of A549-DDP cells. The results showed no significant cytotoxicity in $\mathrm{CP_8K_4}$ and the MF-DDS (**Fig. S10A**). Also, this MF-DDS has low cytotoxicity in the membrane fusion mediated by the coiled-coil lipopeptides, and the cell viability can still be maintained above 90 % at the concentration of 1000 µg/mL (**Fig. S10B**). Subsequently, to overcome the DDP resistance of the A549-DDP cancer cell model, we loaded DDP into the MF-DDS and the DDP

was delivered in large quantities to the cytoplasm by membrane fusing. Results showed that 13.42-folds increased the killing efficiency of A549-DDP cells after delivering the DDP through membrane fusion (IC $_{50}=1.93~\mu\text{g/mL}$) compared to free DDP (IC $_{50}=25.90~\mu\text{g/mL}$) (Fig. 5A,B & Fig. S4D). Next, we visualized the cell-killing effect in each group using a cell dead-live staining assay, in which Calcein-AM labeled living cells exhibited green fluorescence and PI labeled dead cells exhibited red fluorescence. As shown in Fig. S11, the CP $_8\text{K}_4$ + PLGA-DDP@LB-CP $_8\text{E}_4$ group, led to the highest number of PI-labeled dead cells, with almost all labeled cells. In the control group, nearly no red fluorescence signal was shown.

Afterward, we evaluated the therapeutic efficiency of the MF-DDS under the complicated heterogeneous microenvironments using the 3D DDP-resistant lung cancer cell microspheres model. We processed tissue sections of the administered DDP-resistant microspheres and performed H&E staining, which allowed direct observation of the morphological and tissue structural changes (Fig. 5C). The dense arrangement of cells, like the solid tumor, could be observed in the control group. Meanwhile, the MF-DDS caused cellular damage and apoptosis in the periphery of the cell microspheres, but it could also significantly damage tumor necrosis in the central region of the microspheres. Subsequently, we examined the distribution of living and dead cells in microspheres after the drug was treated with living/dead cell staining. The results showed that PI labeled the dead cells in the microspheres at the center in the control group (Fig. 5D), mainly due to the lack of oxygen and nutrients in the core of microspheres leading to the production of the dead cells. After delivery of the DDP via membrane fusion, a large number of apoptotic cells were labeled, accompanied by a reduction in the proportion of live cells. This result was consistent with the H&E staining and further demonstrated that the membrane fusion systems effectively deliver the DDP drug into the interior of the microspheres and efficiently kill the drug-resistant cancer cells. Subsequently, we quantified apoptotic cells in the DDP-resistant microspheres model using the Annexin V-FITC/PI detection assay. As shown in Fig. 5E,F, the CP8K4 + PLGA-DDP@LB-CP8E4 group induced the most efficient cell apoptosis in the DDP-resistant microspheres by 89.95 \pm 0.28 %, yet other treatment groups with DDP, CP₈K₄ + PLGA-DDP@LB, and PLGA-DDP@LB-CP8E4 just caused cell apoptosis the DDP-resistant microspheres by 20.80 \pm 0.83 %, 24.55 \pm 0.74 %, and 25.33 \pm 0.83 %, respectively. These results indicated that this MF-DDS can effectively induce the apoptosis of DDP-resistant lung cancer cells.

3.6. The MF-DDS combated the DDP-resistant lung cancer and showed high biosafety in vivo

Although in vitro 3D cell microsphere models can best mimic solid tumors in vivo, the complexity of the microenvironment and the presence of many non-target cells make it challenging to apply the MF-DDS in vivo. Therefore, we established the A549-DDP subcutaneous lung cancer model to further investigate the inhibition of proliferation and killing of cancer cells by MF-DDS in vivo (Fig. 6A). After 19 days, there was no significant difference in the relative tumor volume of all control groups (including control, DDP, CP8K4 + PLGA@LB, and PLGA@LB- CP_8E_4 groups), while in the MF-DDS group ($CP_8K_4 + PLGA@LB-CP_8E_4$ group) significantly inhibited the tumor size in vivo (Fig. 6B). Also, the MF-DDS group exhibited a smaller tumor weight of 5.26-folds than free DDP groups and 5.23 to 5.44-folds than that of other NDDs groups (Fig. 6C,D). To further confirm the potential therapeutic effect of MF-DDS in vivo, we performed H&E, Ki67, and tunel staining of tumor tissue sections. H&E staining of tumor tissue sections showed histomorphological changes after treatment, in which MF-DDS severely lysed tumor cells and significantly reduced the density and integrity of the tumor (Fig. 6E). In addition, MF-DDS led to a significant increase in tunel positivity area, indicating that the MF-DDS could effectively induce tumor cell apoptosis in vivo (Fig. 6F,H). Meanwhile, Ki67 protein expression was significantly reduced, suggesting that tumor cell

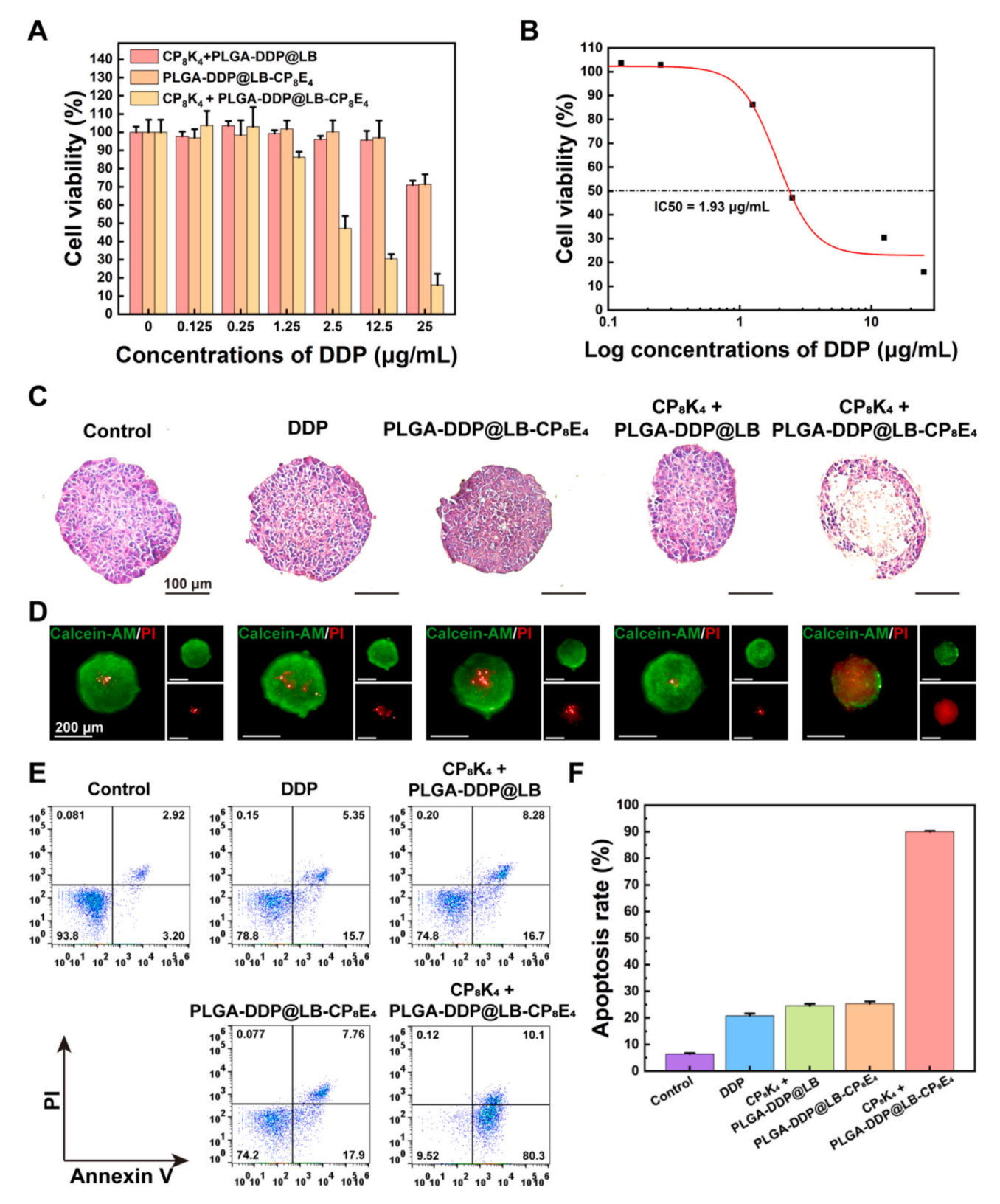


Fig. 5. The MF-DDS against DDP-resistant lung cancer cell model *in vitro*. (A) The cell viability of A549-DDP cells that were incubated with CP₈K₄ for 30 min, and then incubated with PLGA-DDP@LB or PLGA-DDP@LB-CP₈E₄ that loaded with different concentrations of DDP from 0 to 25 μ g/mL for 24 h. (B) The IC₅₀ curve of A549-DDP cells after incubated with CP₈K₄ for 30 min, and then incubated with PLGA-DDP@LB-CP₈E₄ for 24 h. (C) H&E staining of A549-DDP cell microspheres, scale bar = 100 μ m. (D) Calcein-AM/PI living/dead cell staining of A549-DDP cell microspheres, scale bar = 200 μ m. Calcein-AM (green channel, Ex/Em = 494/517 nm), PI (red channel, Ex/Em = 535/617 nm). (E) Annexin V/PI cell apoptosis assay of A549-DDP cell microspheres, and the (F) quantitative analysis of the apoptosis rate in A549-DDP cells microspheres. n = 5, Values shown are mean \pm S.D.

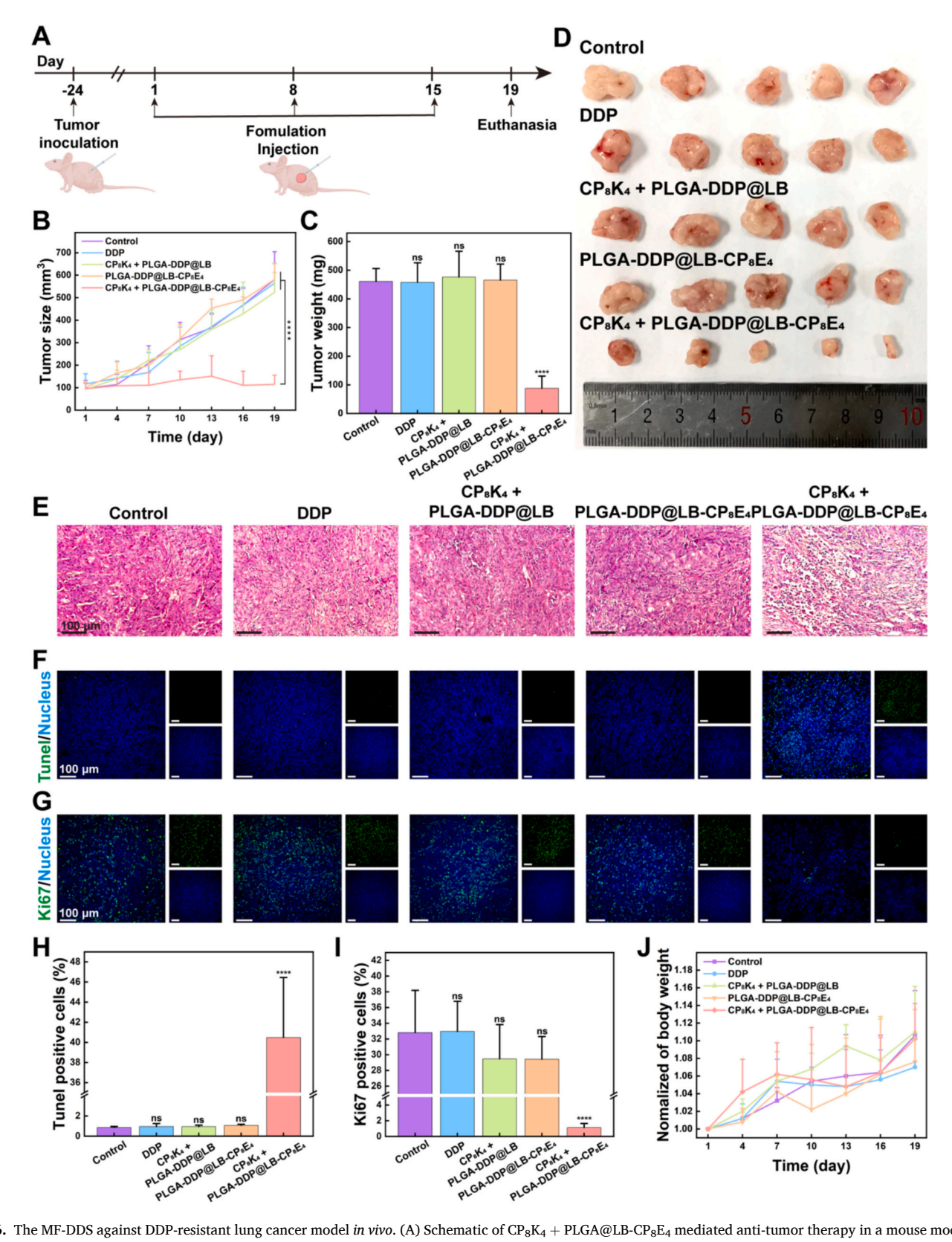


Fig. 6. The MF-DDS against DDP-resistant lung cancer model *in vivo*. (A) Schematic of $CP_8K_4 + PLGA@LB-CP_8E_4$ mediated anti-tumor therapy in a mouse model. (B) The average tumor growth kinetics in different groups. (C) Qualification of excised tumor weight and the (D) representative photographs. (E) The H&E staining of tumor tissue sections. (F) The Tunel staining and (H) qualification of the percentages of tunel positive cells in tumor tissue sections. (G) The immunofluorescence staining of Ki67 and (I) qualification of the percentages of Ki67 positive cells in tumor tissue sections. (J) The body weight changes of mice. Values shown are mean \pm S.D., ****p < 0.0001, vs. Control group, ns indicates no statistical significance. n = 5, scale bar = 100 μ m.

proliferation was inhibited (Fig. 6G,I). Meanwhile, there was no significant difference in the body weights of the mice in each group (Fig. 6J). These results indicated that MF-DDS could efficiently suppress the proliferation and induce apoptosis of DDP-resistant lung cancer cells *in vivo*.

The MF-DDS enabled rapid intracellular drug delivery and excellent cancer cell killing efficiency, it may cause acute toxicity of concern *in vivo*. Thus, we selected 3-folds dose than the pharmacodynamic evaluation portion *in vivo* and then injected MF-DDS without DDP loading using the same injection method and site *in vivo*. The results showed that the body weight and organ index of mice in the MF-DDS group were not significantly different from those in the control group after 48 h (**Fig. S12A,B**). Also, H&E staining of major organs in the area of subcutaneous injections showed no significant histological changes, indicating the safty of this drug delivery system (**Fig. S12C**).

4. Conclusion and discussion

In summary, we constructed a coiled-coil lipopeptide modified lipid coating PLGA nanoparticles for the intracellular delivery of drugs to combat DDP-resistant lung cancer. This membrane fused drug delivery system allows quick drug accumulation in cells via membrane fusion, and exhibited excellent therapeutic efficacy for 13.42-folds reduced IC $_{50}$ value of A549-DDP cells $in\ vito$ and 5.26 folds smaller tumor weight $in\ vivo$ compared with free DDP, which significantly reduced the dose of chemotherapeutic drugs used and effectively reversed tumor resistance. Additionally, the lipid membrane fusion inhibited the gene expression of ABC transporter proteins, including MRP1, MRP2, and ABCG2, at the beginning of 12 or 24 h. This membrane fused drug delivery strategy provides valuable insights into drug-resistant tumor treatment strategies.

Drug resistance of DDP limits its clinical application, where NDDs can help solve the chemoresistance by developing stimuli-responsive and actively targeted, targeting of the tumor microenvironment and immunotherapy, and other novel NDDs. NDDs can be designed to address the resistance mechanism of DDP-resistant that promote the endocytosis of DDP-loaded NDDs in DDP-resistant cancer cells, enhance intracellular DDP accumulation, and combat the DDP-resistant cancer cells. Most NDDs enter the cytoplasm via endocytosis, bypassing the intrinsic transport pathways of DDP, and thus combat the pathway of DDP entering cells through membrane transport proteins (like copper transport proteins CTR1 and CTR2) that showed low levels on the DDPresistant cancer cells [9,40]. However, the endocytosis pathway is inevitably encapsulated by endosomes or/and lysosomes, which can lead to an increased risk of DDP degradation. Our study provided a novel approach that delivered drugs into cells by membrane fusing with cell membrane and could avoid uptake by lysosomes as much as possible, which greatly reduced the risk of DDP degradation showing a major advantage. Furthermore, this MF-DDS could inhibit the expression of efflux receptor genes (including MRP1, MRP2, and ABCG2 highly expressed on the DDP-resistant cancer cells) after the membrane fused with A549-DDP cells, although the expression of MRP2 and ABCG2 genes decreased at 12 h and returned to normal at 24 h, results showed quickly accumulation of drug in cells also reach lethal concentrations, subsequently leading the cell apoptosis in vivo. Altogether, our MF-DDS could increase DDP entry and lead to high intracellular DDP concentration while inhibiting DDP efflux, improving drug-resistant cancer cell killing efficiency. We believe that this drug delivery strategy shows a promising therapeutic strategy for drug-resistant tumor treatment, and could be combined with some modification strategies such as lipid coatings with chemotaxis-responsive ability, specific targeting ligands modifications, and environmentally responsive nanoparticles or coatings in vivo to realize more anti-drug resistant disease treatments.

CRediT authorship contribution statement

Xi Wang: Writing – original draft, Visualization, Validation, Software, Methodology, Investigation, Formal analysis, Data curation, Conceptualization. Guiquan Liu: Visualization, Validation, Software, Methodology, Data curation. Xueyu Pu: Visualization, Validation, Methodology, Investigation, Data curation. Tangjun Ren: Visualization, Validation, Data curation. Fan Zhang: Methodology. MengJie Shen: Resources, Conceptualization. Yan Zhu: Writing – review & editing, Supervision, Software, Resources. Alexander Kros: Writing – review & editing, Supervision, Resources, Formal analysis, Conceptualization. Jian Yang: Writing – review & editing, Supervision, Software, Resources, Project administration, Funding acquisition, Formal analysis, Conceptualization.

Declaration of competing interest

The authors declare that they have no known competing financial interests or personal relationships that could have appeared to influence the work reported in this paper.

Data availability

Data will be made available on request.

Acknowledgements

This work was supported by the National Natural Science Foundation of China (No. 82074032, 62231025), the Natural Science Foundation of Tianjin (No. S24ZS03048), and the TUTCM Graduate Research Innovation Project (No. YJSKC-20231009).

Appendix A. Supplementary data

Supplementary data to this article can be found online at https://doi.org/10.1016/j.jconrel.2025.01.004.

References

- [1] F. Bray, M. Laversanne, H. Sung, J. Ferlay, R.L. Siegel, I. Soerjomataram, A. Jemal, Global cancer statistics 2022: GLOBOCAN estimates of incidence and mortality worldwide for 36 cancers in 185 countries, CA Cancer J. Clin. 74 (2024) 229–263.
- [2] S. Rottenberg, C. Disler, P. Perego, The rediscovery of platinum-based cancer therapy, Nat. Rev. Cancer 21 (2021) 37–50.
- [3] P.B. Tchounwou, S. Dasari, F.K. Noubissi, P. Ray, S. Kumar, Advances in our understanding of the molecular mechanisms of action of cisplatin in cancer therapy, J. Exp. Pharmacol. 13 (2021) 303–328.
- [4] L. Wang, Y. Xie, S. Myrzagali, W. Pu, E. Liu, Metal ions as effectual tools for cancer with traditional Chinese medicine, Acupunct. Herb. Med. 3 (2023) 296–308.
- [5] F. Li, Z. Zheng, W. Chen, D. Li, H. Zhang, Y. Zhu, Q. Mo, X. Zhao, Q. Fan, F. Deng, C. Han, W. Tan, Regulation of cisplatin resistance in bladder cancer by epigenetic mechanisms, Drug Resist. Updat. 68 (2023) 100938.
- [6] C. Zhang, C. Xu, X. Gao, Q. Yao, Platinum-based drugs for cancer therapy and antitumor strategies, Theranostics 12 (2022) 2115–2132.
- [7] R. Liu, Z. Liu, C. Yu, Y. Zhang, X. Feng, Q. Zhang, W. Dang, X. Jia, B. Jia, J. He, B. Xing, Z. Li, H. Li, X. Guo, D. Kebebe, J. Pi, P. Guo, Construction of curcuminloaded micelles and evaluation of the antitumor effect based on angiogenesis, Acupunct. Herb. Med. 3 (2023) 343–356.
- [8] G. Vigueras, G. Gasser, Anticancer platinum-based photo-oxidants in a new light, Nat. Chem. 15 (2023) 896–898.
- [9] M.J. Mitchell, M.M. Billingsley, R.M. Haley, M.E. Wechsler, N.A. Peppas, R. Langer, Engineering precision nanoparticles for drug delivery, Nat. Rev. Drug Discov. 20 (2021) 101–124.
- [10] Y. Han, P. Wen, J. Li, K. Kataoka, Targeted nanomedicine in cisplatin-based cancer therapeutics, J. Control. Release 345 (2022) 709–720.
- [11] Q. Zhang, G. Kuang, L. Zhang, Y. Zhu, Nanocarriers for platinum drug delivery, J. Biomed. Technol. 2 (2023) 77.
- [12] Z.T. Cao, Z.Y. Chen, C.Y. Sun, H.J. Li, H.X. Wang, Q.Q. Cheng, Z.Q. Zuo, J.L. Wang, Y.Z. Liu, Y.C. Wang, J. Wang, Overcoming tumor resistance to cisplatin by cationic lipid-assisted prodrug nanoparticles, Biomaterials 94 (2016) 9.
- [13] C. He, C. Poon, C. Chan, S.D. Yamada, W. Lin, Nanoscale coordination polymers codeliver chemotherapeutics and siRNAs to eradicate tumors of cisplatin-resistant ovarian cancer, J. Am. Chem. Soc. 138 (2016) 6010.

- [14] G.J. Doherty, H.T. McMahon, Mechanisms of endocytosis, Annu. Rev. Biochem. 78 (2009) 857
- [15] J. Yang, Y. Shimada, R.C. Olsthoorn, B.E. Snaar-Jagalska, H.P. Spaink, A. Kros, Application of coiled coil peptides in liposomal anticancer drug delivery using a zebrafish xenograft model, ACS Nano 10 (2016) 7428.
- [16] J. Yang, A. Bahreman, G. Daudey, J. Bussmann, R.C. Olsthoorn, A. Kros, Drug delivery via cell membrane fusion using lipopeptide modified liposomes, ACS Cent. Sci. 2 (2016) 621.
- [17] J. Yang, J. Tu, G.E.M. Lamers, R.C.L. Olsthoorn, A. Kros, Membrane fusion mediated intracellular delivery of lipid bilayer coated mesoporous silica nanoparticles, Adv. Healthc. Mater. 6 (2017) 1700759.
- [18] H.R. Zope, F. Versluis, A. Ordas, J. Voskuhl, H.P. Spaink, A. Kros, In vitro and in vivo supramolecular modification of biomembranes using a lipidated coiled-coil motif, Angew. Chem. Int. Edit. 52 (2013) 14247.
- [19] F. Zahednezhad, P. Zakeri-Milani, J. Shahbazi Mojarrad, H. Valizadeh, The latest advances of cisplatin liposomal formulations: essentials for preparation and analysis, Expert Opin. Drug Deliv. 17 (2020) 523.
- [20] F. Danhier, E. Ansorena, J.M. Silva, R. Coco, A. Le-Breton, V. Préat, PLGA-based nanoparticles: an overview of biomedical applications, J. Control. Release 161 (2012) 505–522.
- [21] X. Pu, Y. Wang, X. Wang, X. Sang, M. Jiang, D. Qi, X. Zhao, R. Chen, J. Li, X. Liu, Z. Liu, J. Yang, Lipids extracted from mycobacterial membrane and enveloped PLGA nanoparticles for encapsulating antibacterial drugs elicit synergistic antimicrobial response against mycobacteria, Mol. Pharm. 21 (2024) 2238.
- [22] X. Wang, Y. Wang, Z. Xue, W. Wan, Y. Li, H. Qin, Y. Zhu, F. Tian, J. Yang, Magnetic liposome as a dual-targeting delivery system for idiopathic pulmonary fibrosis treatment, J. Colloid Interface Sci. 636 (2023) 388.
- [23] S.J. Shirbin, K. Ladewig, Q. Fu, M. Klimak, X. Zhang, W. Duan, G.G. Qiao, Cisplatin-induced formation of biocompatible and biodegradable polypeptidebased vesicles for targeted anticancer drug delivery, Biomacromolecules 16 (2015) 2463.
- [24] E. Jouan, V.M. Le, A. Mayati, C. Denizot, Y. Parmentier, O. Fardel, Evaluation of P-glycoprotein inhibitory potential using a rhodamine 123 accumulation assay, Pharmaceutics 8 (2016) 12.
- [25] J. Adler, I. Parmryd, Quantifying colocalization by correlation: the Pearson correlation coefficient is superior to the Mander's overlap coefficient, Cytom. Part A 77 (2010) 733.
- [26] K.W. Dunn, M.M. Kamocka, J.H. McDonald, A practical guide to evaluating colocalization in biological microscopy, Am. J. Phys. Cell Physiol. 300 (2011) C723

- [27] Y. Zeng, M. Shen, A. Singhal, G.J.A. Sevink, N. Crone, A.L. Boyle, A. Kros, Enhanced liposomal drug delivery via membrane fusion triggered by dimeric coiled-coil peptides, Small 19 (2023) e2301133.
- [28] W.R. Algar, N. Hildebrandt, S.S. Vogel, I.L. Medintz, FRET as a biomolecular research tool - understanding its potential while avoiding pitfalls, Nat. Methods 16 (2019) 815.
- [29] R. Mattioli, A. Ilari, B. Colotti, L. Mosca, F. Fazi, G. Colotti, Doxorubicin and other anthracyclines in cancers: activity, chemoresistance and its overcoming, Mol. Asp. Med. 93 (2023) 101205.
- [30] C. Riccardi, I. Nicolett, Analysis of apoptosis by propidium iodide staining and flow cytometry, Nat. Protoc. 1 (2006) 1458.
- [31] L. Neufeld, E. Yeini, S. Pozzi, R. Satchi-Fainaro, 3D bioprinted cancer models: from basic biology to drug development, Nat. Rev. Cancer 22 (2022) 679.
- [32] B. Chellan, C.A. Reardon, G.S. Getz, Enzymatically modified low-density lipoprotein promotes foam cell formation in smooth muscle cells via macropinocytosis and enhances receptor-mediated uptake of oxidized low-density lipoprotein, Arterioscl. Throm. Vas. 36 (2016) 1101.
- [33] H. Akita, K. Enoto, T. Masuda, H. Mizuguchi, T. Tani, H. Harashima, Particle tracking of intracellular trafficking of octaarginine-modified liposomes: a comparative study with adenovirus, Mol. Ther. 18 (2010) 955.
- [34] M. Otręba, L. Kośmider, A. Rzepecka-Stojko, Antiviral activity of chlorpromazine, fluphenazine, perphenazine, prochlorperazine, and thioridazine towards RNAviruses, Eur. J. Pharmacol. 887 (2020) 173553.
- [35] J. Lee, M. Twomey, C. Machado, G. Gomez, M. Doshi, A.J. Gesquiere, J.H. Moon, Caveolae-mediated endocytosis of conjugated polymer nanoparticles, Macromol. Biosci. 13 (2013) 913.
- [36] R.W. Robey, K.M. Pluchino, M.D. Hall, A.T. Fojo, S.E. Bates, M.M. Gottesman, Revisiting the role of ABC transporters in multidrug-resistant cancer, Nat. Rev. Cancer 18 (2018) 452.
- [37] M.S. Pote, R.N. Gacche, ATP-binding cassette efflux transporters and MDR in cancer, Drug Discov. Today 28 (2023) 103537.
- [38] Q. Huang, Q. Wang, D. Li, X. Wei, Y. Jia, Z. Zhang, B. Ai, X. Cao, T. Guo, Y. Liao, Co-administration of 20(S)-protopanaxatriol (g-PPT) and EGFR-TKI overcomes EGFR-TKI resistance by decreasing SCD1 induced lipid accumulation in non-small cell lung cancer, J. Exp. Clin. Cancer Res. 38 (2019) 129.
- [39] M. Bacci, N. Lorito, A. Smiriglia, A. Morandi, Fat and furious: lipid metabolism in antitumoral therapy response and resistance, Trends Cancer 7 (2021) 198–213.
- [40] M.D. Hall, M. Okabe, D.W. Shen, X.J. Liang, M.M. Gottesman, The role of cellular accumulation in determining sensitivity to platinum-based chemotherapy, Annu. Rev. Pharmacol. Toxicol. 48 (2008) 495.